Anisotropic Permittivity and Attenuation Extraction From Propagation Constant Measurements Using an Anisotropic Full-Wave Green's Function Solver for Coplanar Ferroelectric Thin-Film Devices

Clifford M. Krowne, *Senior Member, IEEE*, Maurice Daniel, Steven W. Kirchoefer, *Member, IEEE*, and Jeffrey M. Pond, *Member, IEEE*

***Abstract*—In this paper, a full-wave spectral-domain integral-equation technique is used to study double substrate layer coplanar devices with the ferroelectric thin film adjacent to the conductor guiding interfacial surface. The Green's function is used in the anisotropic situation for anisotropic permittivities. In examining specific laboratory data, going from an unbiased static electric field to the biased case, the permittivity tensor is allowed to go from a unity tensor to a uniaxial one. Consistent with this permittivity tensor behavior, the attenuation trend with frequency and its amplitude is also found.**

***Index Terms*—Anisotropic, attenuation, coplanar, electromagnetic propagation, experimental data, ferroelectric, Green's function, simulations, spectral-domain code, thin-film devices.**

I. Introduction

DETERMINATION of ferroelectric thin-film permittivities has relied upon the measurement of interdigitated capacitor values at several hundred megahertz to a few gigahertz [1], [2]. This is a reasonably reliable way to assess the actual permittivity values. However, it would be nice to be able to extract the permittivity values when the frequency increases significantly, and this appears to be promising for transmission-line devices, which rely upon wave propagation down a length of uniform transmission-line structure [3].

In this paper, we will report on the theoretical procedure to extract the tensor aspects of the permittivity of the ferroelectric, due to either intrinsic or imposed anisotropy, the simulation technique developed relying upon using a full-wave spectral-domain integral-equation method using an anisotropic Green's function [4], [5], and numerical results based upon recent fabricated and measured devices made from $Ba_x\ Sr_{1-x}TiO_3$ material. General theoretical discussions of various tensors for ferroelectric and ferromagnetic materials, as well as other crystals, and their spatial rotations are available elsewhere [6], [7]. Extraction issues are examined there also [6], [7].

Manuscript received September 19, 2000. This work was supported in part by the Office of Naval Research and by the Defense Advanced Projects Agency under the Frequency Agile Materials for Electronics Program.

C. M. Krowne, S. W. Kirchoefer, and J. M. Pond are with the Microwave Technology Branch, Electronics Science and Technology Division, Naval Research Laboratory, Washington, DC 20375-5347 USA.

M. Daniel is with the DCS Corporation, Alexandria, VA 22314 USA.

Publisher Item Identifier S 0018-9480(02)01166-3.

The various loss contributions will also be evaluated (beyond what was presented earlier on just permittivity [8][1]), including the ohmic (conductor loss) contribution, which appears to be significant compared to other possible loss mechanisms. Substrate and ferroelectric bulk loss, characterized by a loss tangent, are treated in a fully self-consistent way in the Green's function construction. Ohmic loss, by the interfacial guiding coplanar metal, is treated in two alternative fashions. Dyadic Green's function element modifications within the self-consistent process or a perturbational ohmic-loss contribution after the self-consistent process, yield the attenuation constant.

II. Ferroelectric Permittivity Tensor

In general, assuming the crystalline principal axes of the ferroelectric film are oriented in the coordinate directions, the permittivity tensor $\overline{\overline{\varepsilon}}$ looks like

$$\overline{\overline{\varepsilon}}(0) = \begin{bmatrix} \varepsilon_{xx}(0) & 0 & 0 \\ 0 & \varepsilon_{yy}(0) & 0 \\ 0 & 0 & \varepsilon_{zz}(0) \end{bmatrix} \tag{1}$$

in the unbiased situation, i.e., $\mathbf{E}_{\text{bias}} = 0$. When bias is applied, $\overline{\overline{\varepsilon}}$ becomes

$$\overline{\overline{\varepsilon}}(\mathbf{E}_{\text{bias}}) = \begin{bmatrix} \varepsilon_{xx}(\mathbf{E}_{\text{bias}}) & 0 & 0 \\ 0 & \varepsilon_{yy}(\mathbf{E}_{\text{bias}}) & 0 \\ 0 & 0 & \varepsilon_{zz}(\mathbf{E}_{\text{bias}}) \end{bmatrix}. \tag{2}$$

Each tensor $\overline{\overline{\varepsilon}}$ element can be a function of each of the three bias field components $E_{i,\text{bias}}$, where $i = x, y, z$. If we assume, for simplicity, diagonal functional projection of the bias field components onto the permittivity tensor $\overline{\overline{\varepsilon}}$ elements, then we find

$$\overline{\overline{\varepsilon}}(\mathbf{E}_{\text{bias}}) = \begin{bmatrix} \varepsilon_{xx}(E_{x,\text{bias}}) & 0 & 0 \\ 0 & \varepsilon_{yy}(E_{y,\text{bias}}) & 0 \\ 0 & 0 & \varepsilon_{zz}(E_{z,\text{bias}}) \end{bmatrix}. \tag{3}$$

This is a form simple enough to allow unique determination of the permittivity tensor $\overline{\overline{\varepsilon}}$ elements from propagation phase constant β data.

[1]Voltage bias labels were inadvertently reversed in Fig. 3.

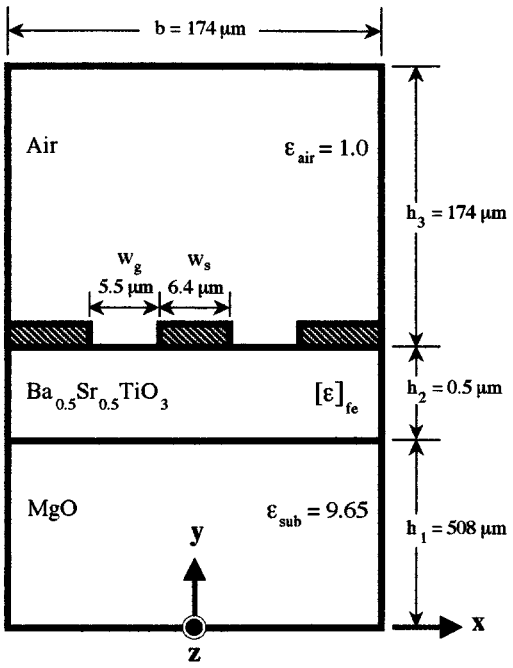

Fig. 1. Cross-sectional diagram of the ferroelectric microwave transmission-line structure with dimensions and permittivities indicated for the $Ba_{0.5}Sr_{0.5}TiO_3$ stoichiometry film over an MgO substrate.

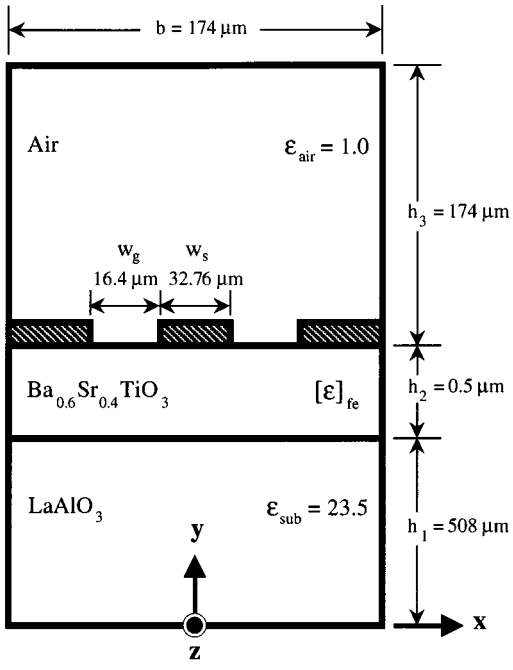

Fig. 2. Cross-sectional diagram of the ferroelectric microwave transmission-line structure with dimensions and permittivities indicated for the $Ba_{0.6}Sr_{0.4}TiO_3$ stoichiometry film over an $LaAlO_3$ substrate.

III. Coplanar Permittivity Tensor Forms

Using the hexagonal perovskite crystalline form for $Ba_xSr_{1-x}TiO_3$ material, with the c-axis parallel to the y-axis and having different properties than in the a- and b-axes directions parallel to the xz-plane and having the same effects, the tensor $\overline{\overline{\varepsilon}}$ looks uniaxial in the unbiased case

$$\overline{\overline{\varepsilon}}(0) = \begin{bmatrix} \varepsilon_{xx}(0) & 0 & 0 \\ 0 & \varepsilon_{yy}(0) & 0 \\ 0 & 0 & \varepsilon_{xx}(0) \end{bmatrix}. \tag{4}$$

This $\varepsilon_{xx} = \varepsilon_{zz}$ equality is broken under bias in the coplanar device, where for the thin films under consideration, $\mathbf{E}_{\text{bias}} \approx E_{x,\,\text{bias}}\hat{x}$ is a reasonable approximation [9]. Thus, the ferroelectric effect makes $\overline{\overline{\varepsilon}}$ become

$$\overline{\overline{\varepsilon}}(E_{\text{bias}}) = \begin{bmatrix} \varepsilon_{xx}(E_{x,\,\text{bias}}) & 0 & 0 \\ 0 & \varepsilon_{yy}(0) & 0 \\ 0 & 0 & \varepsilon_{xx}(0) \end{bmatrix}. \tag{5}$$

In this form, the permittivity tensor is biaxial.

In order to make the extraction of the tensor element values simple and unique, we impose the condition of isotropy upon the unbiased tensor $\overline{\overline{\varepsilon}}$ in (4) to give

$$\overline{\overline{\varepsilon}}(0) = \begin{bmatrix} \varepsilon(0) & 0 & 0 \\ 0 & \varepsilon(0) & 0 \\ 0 & 0 & \varepsilon(0) \end{bmatrix}. \tag{6}$$

When this done, the value of $\varepsilon(0)$ is iterated until the phase propagation constants determined experimentally and numerically agree, i.e., until $\beta_{\text{th}}[\varepsilon(0)] = \beta_{\text{exp}}$. Once this value is on hand, it is assigned to the yy and zz tensor $\overline{\overline{\varepsilon}}$ elements in (5) so that $\varepsilon_{yy} = \varepsilon_{zz} = \varepsilon(0)$, converting (5) into

$$\overline{\overline{\varepsilon}}(E_{x,\,\text{bias}}) = \begin{bmatrix} \varepsilon_{xx}(E_{x,\,\text{bias}}) & 0 & 0 \\ 0 & \varepsilon(0) & 0 \\ 0 & 0 & \varepsilon(0) \end{bmatrix}. \tag{7}$$

Once (7) is available, the process of repeated iteration with ε_{xx}, the unknown to be found, can be started. The iteration process stops when $\beta_{\text{th}}[\varepsilon_{xx}(E_{x,\text{bias}})] = \beta_{\text{exp}}$ has been satisfied. We note here that the dependence of various ferroelectric coplanar cladded structures have been studied for the form (6), with varying $\varepsilon(0)$ and geometric dimensions [10]. These canonical structures do include the direct calculation (versus the reverse extraction procedure to follow below) of the ferroelectric substrate coplanar device type.

IV. Numerical Extraction of Permittivity Tensor Elements

Figs. 1 and 2 show the geometry of the thin-film structures simulated using the full-wave code. The first structure uses $Ba_xSr_{1-x}TiO_3$ with a compositional ratio of $x = 0.5$ over an MgO substrate. The second structure has a compositional ratio of $x = 0.6$ over an $LaAlO_3$ substrate. Both structures have the same size enclosure consisting of perfect electric walls. Box width is $b = 174\ \mu$m, with substrate, ferroelectric film, and air region thicknesses being $h_1 = 508\ \mu$m, $h_2 = 0.5\ \mu$m, and $h_3 = 174\ \mu$m. Relative dielectric constants of the substrates are $\varepsilon_{\text{sub}} = 9.65$ and $\varepsilon_{\text{sub}} = 23.5$ for MgO and $LaAlO_3$, respectively. The center strip width $w_s = 6.4\ \mu$m and slot gap size $w_g = 5.5\ \mu$m for the film over MgO substrate. These numbers are considerably larger for the film over $LaAlO_3$, being $w_s = 32.76\ \mu$m and $w_g = 16.4\ \mu$m.

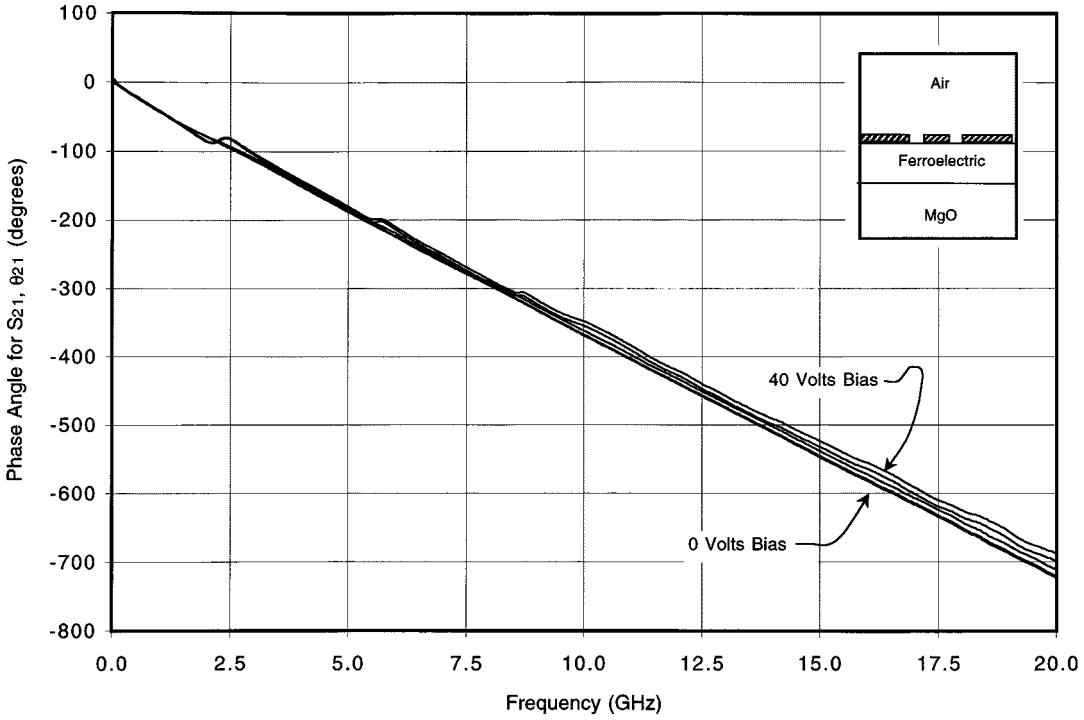

Fig. 3. Phase angle for s_{21}, θ_{21} (degrees), against frequency (in gigahertz) for the $Ba_{0.5}Sr_{0.5}TiO_3$ ferroelectric film over an MgO substrate. $V_{\text{bias}} = 0, 10, 20, 30,$ and 40 V.

Fig. 3 shows a typical phase angle measurement for s_{21}, θ_{21} over the 0–20-GHz frequency range, giving the cumulative phase angle seen by the propagating wave traveling through the device made with MgO. The device prepared over MgO had a length of $L = 0.85$ cm, whereas the device made with $LaAlO_3$ had $L = 1.00$ cm. Measured θ_{21} on a network analyzer has $-180 \leq \theta_{21} \leq 180$, thus, the curves in Fig. 3 have been appropriately modified by the formula $\theta_{21,\text{new}} = \theta_{21,\text{old}} \pm \text{mod}\,360$. Four bias voltage curves are shown here, $V_{\text{bias}} = 0, 10, 20, 30,$ and 40 V (measurements were also made at the reverse voltages, but they are neither provided, nor necessary for the following analysis).

To make a comparison to the simulation results available from the full-wave code, θ_{21} is converted into a normalized propagation constant, This is done by using the simple formula

$$\overline{\beta} = \theta_{21}/[Lk_0] \tag{8}$$

where k_0 = the free-space propagation constant. Note that, to use the full-wave code, the number of basis functions, used to expand the x and z components of the electric field at the interface where the guiding slots exist, is set to $n_x = n_z = 3$ and that the number of Fourier spectral terms $n = 200$.

These new results are plotted in Fig. 4, which shows the two cases $V_{\text{bias}} = 0$ V and 40 V. The permittivity extraction method, discussed in the final section, based upon (6) and (7), has been applied at 10 GHz on this figure. (All the loss mechanisms are turned off in this section, in order to focus on the main physical characteristic of ferroelectric devices, permittivity modification. Loss contribution in relation to the phase behavior, and its affects on the permittivity tensor are covered in a later section.) The top curve for $V_{\text{bias}} = 0$ V has a higher slowing $\overline{\beta} = 3.614$ than the lower curve, and we expect its nominal dielectric constant value to be bigger. This is the case as seen from the determined scalar permittivity value $\varepsilon(0) = 123.9$. For the lower curve, $\overline{\beta} = 3.413$, which yields a permittivity tensor $\overline{\overline{\varepsilon}}$ of

$$\overline{\overline{\varepsilon}}(V_{\text{bias}} = 40\,\text{V}) = \begin{bmatrix} 100.2 & 0 & 0 \\ 0 & 123.9 & 0 \\ 0 & 0 & 123.9 \end{bmatrix}. \tag{9}$$

Electric-field value associated with this tensor solution is found from $E_{x,\text{bias}} = V_{\text{bias}}/w_g = 47.06$ V/cm. It is the electric-field value that is the fundamental quantity, not potential difference, since it directly affects the permittivity behavior of the ferroelectric material film.

Obviously, it is possible to do the previous calculation at each measured frequency point, allowing a plot of the $\overline{\overline{\varepsilon}}$ tensor elements. Since it is the ε_{xx} element that varies, it alone can be plotted versus frequency. Its value will be fairly flat since the curves in Fig. 4 are fairly flat. Variation over f will be due to experimental error, small film material variation over the device surface, and unwanted external and extraneous circuit effects. Since the coplanar device at these dimensions is an extremely low dispersive structure, we do not expect fundamental frequency variation behavior unless the material itself displays such behavior. It is possible to incorporate such material dispersive behavior into the $\overline{\overline{\varepsilon}}$ tensor, although we have not done that in this paper.

Finally, in Fig. 5, a typical phase angle measurement for s_{21}, θ_{21} over the 0–20-GHz frequency range is shown, giving the cumulative phase angle seen by the propagating wave traveling through the device made with $LaAlO_3$. Fig. 6 shows the normalized propagation constant $\overline{\beta}$ results for the device made with an

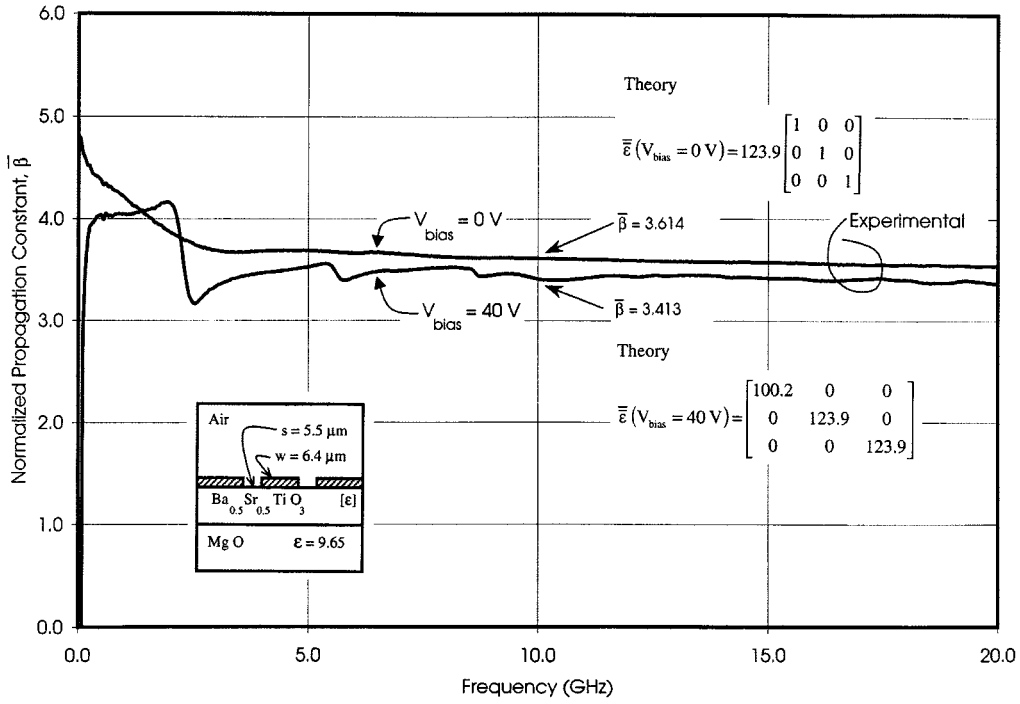

Fig. 4. Normalized propagation constant $\overline{\beta}$ for experiment versus frequency for the $Ba_{0.5}Sr_{0.5}TiO_3$ ferroelectric film over an MgO substrate. Two of the bias voltages are used from Fig. 3, $V_{\rm bias} = 0, 40$ V. $\varepsilon_{\rm sub} = 9.65$ and $\varepsilon_{\rm air} = 1$. Theoretically determined points are shown with the associated permittivity tensor $\overline{\overline{\varepsilon}}$ at 10 GHz. Box width $b = 174$ μm. Thicknesses of the three device layers are $h_1 = 508$ μm, $h_2 = 0.5$ μm, and $h_3 = 174$ μm. Strip width is $w_s = 6.4$ μm and slot gap size $w_g = 5.5$ μm.

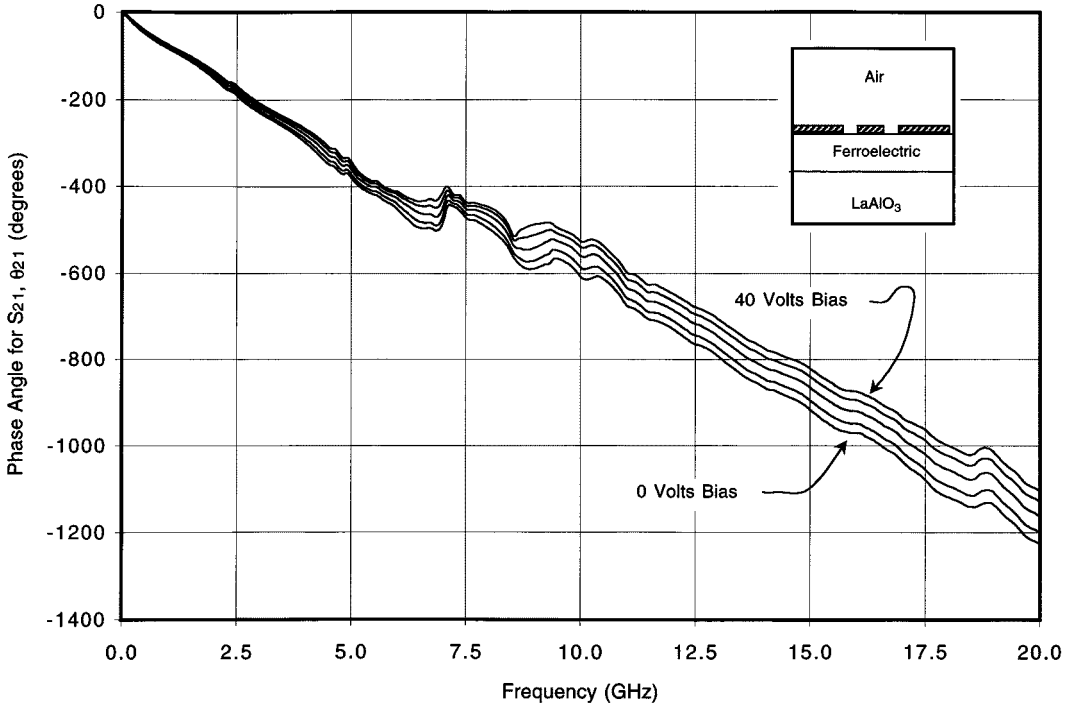

Fig. 5. Phase angle for s_{21}, θ_{21} (degrees), against frequency (in gigahertz) for the $Ba_{0.6}Sr_{0.4}TiO_3$ ferroelectric film over an $LaAlO_3$ substrate. $V_{\rm bias} = 0, 10, 20, 30,$ and 40 V.

$LaAlO_3$ substrate over the 10–20-GHz region. Dielectric constant is much higher for this device with the scalar permittivity $\varepsilon(0) = 723.0$ found from $\overline{\beta}_{\rm th}[\varepsilon(0)] = \overline{\beta}_{\rm exp}$ at $V_{\rm bias} = 0$ V. A solution was obtained as the upper flat line indicates in Fig. 6 ($\overline{\beta}_{\rm th}[V = 0] = 5.110$), while the experimental curve displays some mild oscillatory character. (Note also that this line is the rms average over the band of the experimental data.) The theoretical $\overline{\beta}_{\rm th}$ goes through the average value of the ex-

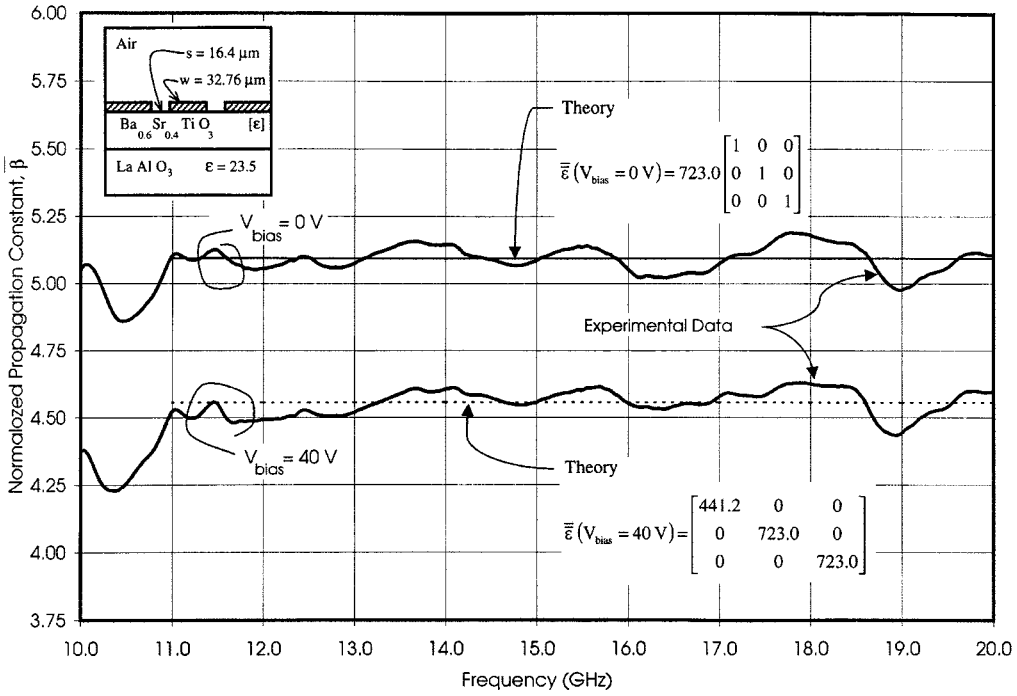

Fig. 6. Normalized propagation constant $\overline{\beta}$ for experiment versus frequency for the $Ba_{0.6}Sr_{0.4}TiO_3$ ferroelectric film over an $LaAlO_3$ substrate. $V_{\rm bias} = 0, 40$ V. $\varepsilon_{\rm sub} = 23.5$ and $\varepsilon_{\rm air} = 1$. Theoretically determined average lines are shown with the associated permittivity tensor $\overline{\overline{\varepsilon}}$ over the 11–20-GHz band. Box width $b = 174$ μm. Thicknesses of the three device layers are $h_1 = 508$ μm, $h_2 = 0.5$ μm, and $h_3 = 174$ μm. Strip width is $w_s = 32.76$ μm and slot gap size $w_g = 16.4$ μm.

perimental data $\overline{\beta}_{\rm exp}$ over the frequency range studied. For the lower curve ($\overline{\beta}_{\rm th}[V = 40] = 4.576$), where $V_{\rm bias} = 40$ V ($E_{x,\rm bias} = 40$ V/cm), the permittivity tensor $\overline{\overline{\varepsilon}}$ is found to be

$$\overline{\overline{\varepsilon}}(V_{\rm bias} = 40\ {\rm V}) = \begin{bmatrix} 441.2 & 0 & 0 \\ 0 & 723.0 & 0 \\ 0 & 0 & 723.0 \end{bmatrix}. \tag{10}$$

V. Attenuation Modeling

Fig. 7 provides the corrected insertion-loss measurement $|s_{21}|_{\rm corr}$ in decibels, over the 0–20-GHz frequency range for the MgO substrate device. Four bias voltage curves are shown, $V_{\rm bias} = 0, 10, 20, 30$, and 40 V. Here,

$$|s_{21}|_{\rm corr} = \left[\frac{|s_{21}|^2}{1 - |s_{11}|^2}\right]^{1/2} \tag{11}$$

so that the insertion-loss value of $|s_{21}|$ must be

$$|s_{21}|_{\rm corr}({\rm dB}) = 10\log_{10}(|s_{21}|^2_{\rm corr}). \tag{12}$$

This value is related to the attenuation constant of the device $\alpha = \alpha_{\rm exp}$ by the power relationship

$$P = P_0 e^{-2\alpha L} \tag{13}$$

where P_0 is the injected power and $P = P(L)$ is the power exiting the device. The relationship between (12) and (13) is

$$|s_{21}|_{\rm corr} = \sqrt{\frac{P}{P_0}}. \tag{14}$$

Combining (13) and (14) gives us the experimental attenuation constant $\alpha_{\rm exp}$

$$\alpha_{\rm exp} = -\frac{|s_{21}|_{\rm corr}({\rm dB})}{20L\log_{10} e}. \tag{15}$$

Again, as we have done earlier, this component of the propagation constant is converted into a normalized value by the simple prescription

$$\overline{\alpha} = \frac{\alpha}{k_0} \tag{16}$$

which is what the code works with. $\alpha_{\rm exp}$ in decibels/millimeter is plotted $[-|s_{21}|_{\rm corr}({\rm dB})/L({\rm mm})]$ in Fig. 8 for the two cases $V_{\rm bias} = 0$ V and 40 V for the MgO substrate.

Loss in the substrate is accounted for by an estimated loss-tangent value $\tan\delta = 1.8 \times 10^{-4}$ at room temperature for MgO. Loss in the ferroelectric material is thought in this experimental device material to be roughly $\tan\delta = 1.0 \times 10^{-2}$. The code ($n_x = n_z = 3$ and $n = 200$) was compared to [11], which is also a full-wave calculation, for dielectric-loss evaluation and found to agree within 1%—the test case was microstrip with width $2w = 0.500$ mm, substrate height $d = 0.500$ mm, relative dielectric constant $\varepsilon_{r1} = 10.0$, box width $= 2a = 20$ mm, box height above substrate (air region) $= h = 19.5$ mm, and $\tan\delta = 2.0 \times 10^{-4}$ and 1.0×10^{-1} (notation used from [11]—note that, in this reference, an approximate two-term expansion was used for surface current J_{sz} with $J_{sx} = 0$).

Loss due to the interfacial conductor metal, made of pure silver $t = 1.5 \times 10^{-6}$ m $= 1.5$-μm thick with a resistivity of

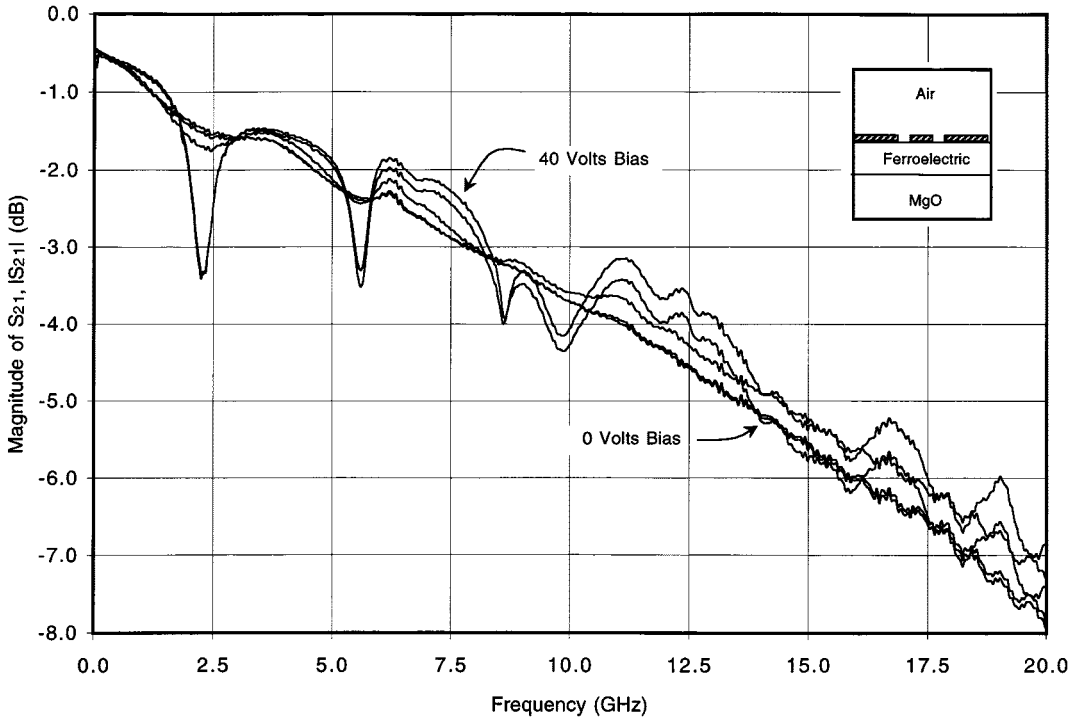

Fig. 7. Corrected insertion loss $|s_{21}|_{\rm corr}$ in decibels, against frequency (in gigahertz) for the $Ba_{0.5}Sr_{0.5}TiO_3$ ferroelectric film over an MgO substrate. $V_{\rm bias} = 0, 10, 20, 30,$ and 40 V.

$\rho = 1.629 \times 10^{-6}\ \Omega \cdot$ cm, is modeled by two separate approaches. The first approach realizes that to include the effects of conductor loss self-consistently in the determination of β requires that the Green's function algorithm be altered. This is done by modifying the impedance Green's function diagonal elements G_{ii}, $i = x, z$ to read

$$G'_{ii} = G_{ii} - G_s. \tag{17}$$

It is known that a simple $G_{s1} = 1/(\sigma t)$ form [12] for a microstrip will estimate the magnitude of the effect, but not the frequency dependence (α declines slightly with f, whereas $\alpha_{\rm exp}$ increases). (Note that, in [12], t and ρ_c ought to read $t = 0.5\ \mu$m and $\rho_c = 2.44 \times 10^{-6}\ \Omega \cdot$ cm $= 2.44\ \mu\Omega \cdot$ cm and this will yield all the shown magnitudes and frequency curve dependencies in that paper.) Modification of this to be $G_{s2} = A\sqrt{f}G_{s1}$ for a microstrip will explicitly inject the known skin-effect surface-resistance dependence on frequency, but it does not reproduce the $\alpha_{\rm exp}$, although it does increase with frequency and, thus, is a much more favorable result [12] ([12, eq. (9)] uses f in gigahertz units and A should be $A = 0.287$). However, using a $G_{s3} = [1/(\sigma\delta)]y\coth(yt/\delta)$ form, where $y = 1$ or $1 + j$ (for resistive or complex surface impedance), which is consistent with earlier work of ours in kinetic inductance effects for superconducting transmission lines [13] and is the form found in [14] for microstrip lines, does yield agreement (within a few percent using $\tan\delta = 4.0 \times 10^{-4}$) with experimental work [15].

Using this knowledge of the dyadic surface impedance form for microstrip, and accounting for the substantial amount of field lines that couple between and penetrate laterally into the coplanar arrangement of metallization, we have chosen the general form

$$G_{s3} = \frac{1}{\sigma w_{\rm eff}}\left\{(1+j)\frac{t}{4\delta} + c(f)\frac{w_{cs}}{w_{cs}+2w_{\rm slot}} \cdot\left[\frac{(1+j)w_{cs}/\delta}{\tanh[(1+j)w_{cs}/\delta]}\right]\right\} \tag{18}$$

where

$$c(f) = c_1\left(\frac{f}{f_0}\right)^v \quad \delta = \frac{1}{\sqrt{\pi f\mu_0\sigma}}. \tag{19}$$

In (18), the first factor handles the resistance contribution to the impedance, with $w_{\rm eff}$ being the effective coplanar metal width. The next curly-bracketed factor handles both the finite thickness and/or width of the metal (comparison made to the skin depth), and the frequency variation. The first term in the brackets accounts for the interfacial coplanar ground planes. The second term accounts for the center conductor strip of width w_{cs} offset from the interfacial ground planes by slot widths $w_{\rm slot}$ (square-bracketed form of the second factor in this term is similar to microstrip form in [14], with t replaced by w_{cs}).

For the coplanar device, which we model as two coupled slots, with the fields in the interfacial slot locations expanded in a complete set of basis functions, we need the admittance Green's function, which has been shown in [16] to be

$$G'_{\rm ad} = \frac{1}{\det G'}\begin{bmatrix} G'_{zz} & -G'_{xz} \\ -G'_{zx} & G'_{xx}\end{bmatrix} \tag{20}$$

where

$$\det G' = G'_{xx}G'_{zz} - G'_{xz}G'_{zx}. \tag{21}$$

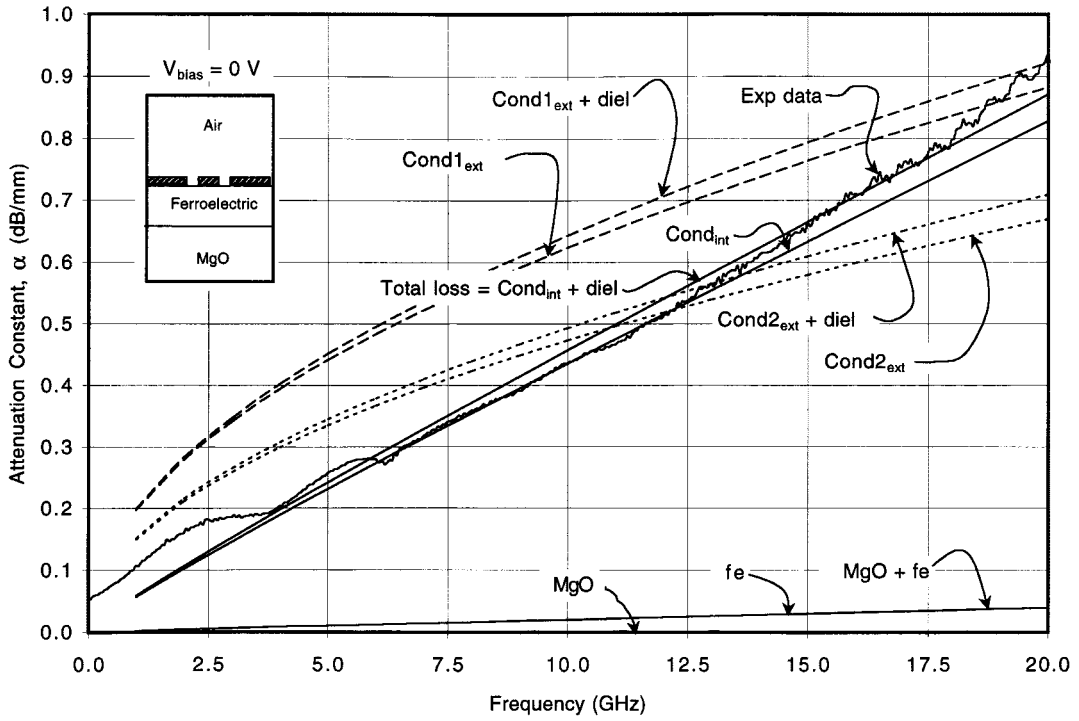

(a)

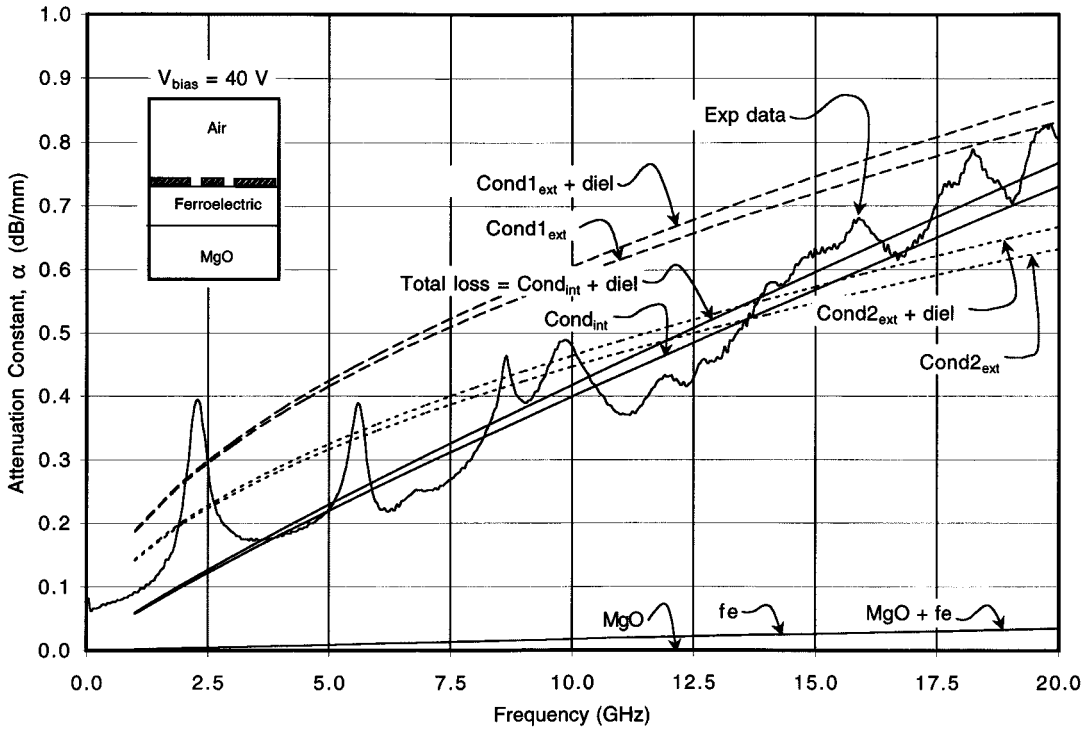

(b)

Fig. 8. Laboratory measured $\alpha_{\rm exp}$ is plotted for the two cases: (a) $V_{\rm bias} = 0$ V and (b) 40 V for the $Ba_{0.5}Sr_{0.5}TiO_3$ ferroelectric film over an MgO substrate. Theoretical attenuative results [$\alpha_{\rm th} = \overline{\alpha}_{\rm th} k_0 (20 \log_{10} e)$] are shown too for only substrate loss $\alpha_{\rm sub}$, thin-film ferroelectric bulk loss $\alpha_{\rm fe}$, both of these bulk effects $\alpha_{\rm sub+fe}$, only the ohmic loss using the internal self-consistent formula (18) $\alpha_{\rm cond,\,in}$, only the ohmic loss using either of the external perturbational formulas (22) [labeled $\rm Cond1_{ext}$] or (35) [labeled $\rm Cond2_{ext}$] $\alpha_{\rm cond,\,ext}$, total loss $\alpha_{\rm tot,\,ext}$, which includes the ohmic loss using either of the external perturbational formulas (22) or (35) and both the dielectric layer loss parts, and the total loss $\alpha_{\rm tot,\,in}$, which includes the ohmic loss using the internal self-consistent formula (18) and both the dielectric layer loss parts.

For the second approach, which utilizes a perturbational method, we rely on the available formulas for coplanar waveguide, which are both limited to being only strictly valid for the fundamental mode (or modes) and are not quite descriptive of the multilayered problem we are handling. However, we hope they will give some realistic indication of the magnitude of the ohmic loss expected and the frequency dependence. The first formula, which arises from the application of Wheeler's incre-

mental inductance rule (we retain the notion of the reference and associate with our notion afterwards) [17], gives loss in decibels/millimeter (W, S, and t in millimeters) as

$$\alpha_{\text{cond, ext}} = 4.88\times 10^{-4} R_s \varepsilon_{re} Z_{ocp} \frac{P'}{W\pi}\left(1+\frac{S}{W}\right) \cdot\left\{\frac{\frac{1.25}{\pi}\ln\frac{4\pi S}{t}+1+\frac{1.25t}{\pi S}}{\left[2+\frac{S}{W}-\frac{1.25t}{\pi W}\left(1+\ln\frac{4\pi S}{t}\right)\right]^2}\right\} \tag{22}$$

where

$$R_s = \sqrt{\pi f \mu_0 \rho} \tag{23}$$

$$P' = \begin{cases} \dfrac{k}{(1-k')(k')^{3/2}}\left[\dfrac{K(k)}{K'(k)}\right]^2, & 0\le k\le 0.707 \\ \dfrac{1}{(1-k)\sqrt{k}}, & 0.707\le k\le 1.0 \end{cases} \tag{24}$$

$$Z_{ocp} = \frac{30\pi}{\sqrt{\varepsilon_{re}^t}}\frac{K'(k_e)}{K(k_e)} \tag{25}$$

$$\varepsilon_{re}^t = \varepsilon_{re} - \frac{0.7(\varepsilon_{re}-1)t/W}{[K(k)/K'(k)]+0.7t/W} \tag{26}$$

$$k_e = \frac{S_e}{S_e+2W_e} \tag{27}$$

$$S_e = S+\Delta \tag{28}$$

$$W_e = W-\Delta \tag{29}$$

$$\Delta = \frac{1.25t}{\pi}\left[1+\ln\left(\frac{4\pi S}{t}\right)\right] \tag{30}$$

$$k = \frac{S}{S+2W} \tag{31}$$

$$k' = \sqrt{1-k^2} \tag{32}$$

$$K'(k) = K(k') \tag{33}$$

$$\frac{K(k)}{K'(k)} = \begin{cases} \left[\dfrac{1}{\pi}\ln\left(2\dfrac{1+\sqrt{k'}}{1-\sqrt{k'}}\right)\right]^{-1}, & 0\le k\le 0.707 \\ \dfrac{1}{\pi}\ln\left(2\dfrac{1+\sqrt{k}}{1-\sqrt{k}}\right), & 0.707\le k\le 1.0 \end{cases}. \tag{34}$$

These equations allow for the slight change of the coplanar middle strip ($S = w_s$) width or the gaps to the ground metal ($W = w_g$) due to the effects of fringing fields associated with the finite metal thickness t. The ratio of the complete elliptic function of the first kind to its complementary function is given by (34) with a reported accuracy of better than one part in 10^5 in [17], but with the intermediate transition region changed from 0.7 to 0.707, the accuracy is reported to be within three parts in 10^6 in [18].

The second formula, based upon the work done by Owyang and Wu, Tuncer *et al.*, and Ghione, and provided in [18], used a direct approach to finding the conductor loss for a finite metallization thickness t. Power dissipated in the line through conformal mapping of the current density in the finite metal thickness coplanar-waveguide structure was evaluated. Attenuation loss in decibels/millimeter (with a, b, and t in millimeters) is

$$\alpha_{\text{cond, ext}} = \frac{8.68R_s\sqrt{\varepsilon_{re}}}{480\pi K(k_1)K'(k_1)(1-k_1^2)} \cdot\left\{\frac{1}{a}\left[\pi+\ln\left(\frac{8\pi a}{t}\frac{1-k_1}{1+k_1}\right)\right] +\frac{1}{b}\left[\pi+\ln\left(\frac{8\pi b}{t}\frac{1-k_1}{1+k_1}\right)\right]\right\} \tag{35}$$

where

$$a = S/2$$
$$b = (S+2W)/2 \tag{36}$$

$$K(k) = \begin{cases} \dfrac{\pi}{2}\left\{1+2\dfrac{k^2}{8}+9\left(\dfrac{k^2}{8}\right)^2+50\left(\dfrac{k^2}{8}\right)^3 +306.25\left(\dfrac{k^2}{8}\right)^4+\cdots\right\}, \\ \qquad 0\le k\le 0.707 \\ p+(p-1)\dfrac{k'^2}{4}+\dfrac{9}{4}\left(p-\dfrac{7}{6}\right)\left(\dfrac{k'^2}{4}\right)^2 +\dfrac{25}{4}\left(p-\dfrac{37}{30}\right)\left(\dfrac{k'^2}{4}\right)^3+\cdots, \\ \qquad 0.707\le k\le 1.0 \end{cases} \tag{37}$$

$$p = \ln\left(\frac{4}{k'}\right) \tag{38}$$

and $k_1 = k$ used in the first formula (31) above. Maximum error in (37) occurs at the crossover point $k = 0.707$ and is 0.3%.

Both (22) and (35), which add the perturbative attenuative loss α_{ext} onto the dielectric loss calculated self-consistently $\alpha_{\text{diel, in}}$, can be upgraded somewhat, including any dispersive frequency effects in the effective dielectric constant of the structure, by assigning

$$\varepsilon_{re} = \left(\frac{\beta}{k_0}\right)^2 = \overline{\beta}^2 \tag{39}$$

which is acquired from the self-consistent run of the code. Thus, the total attenuative loss is

$$\alpha_{\text{total}} = \alpha_{\text{diel, in}} + \alpha_{\text{cond, ext}} \tag{40}$$

where

$$\alpha_{\text{diel, in}} = \alpha_{\text{in, bulk}} = \alpha_{\text{sub, layer}} + \alpha_{fe,\text{ thin film}}. \tag{41}$$

We note that the quasi-static coplanar impedance Z_{ocp} in (25) cannot be upgraded by an analytical formula (none are available in the literature) to include frequency variation, but this is not too much of a problem because, for our structures, the dispersion in ε_{re} is slight, and this is expected to carry over to Z_{ocp}.

Fig. 8 plots for the MgO substrate device the theoretical attenuative results

$$\alpha_{\text{th}} = \overline{\alpha}_{\text{th}} k_0 (20\log_{10} e)$$

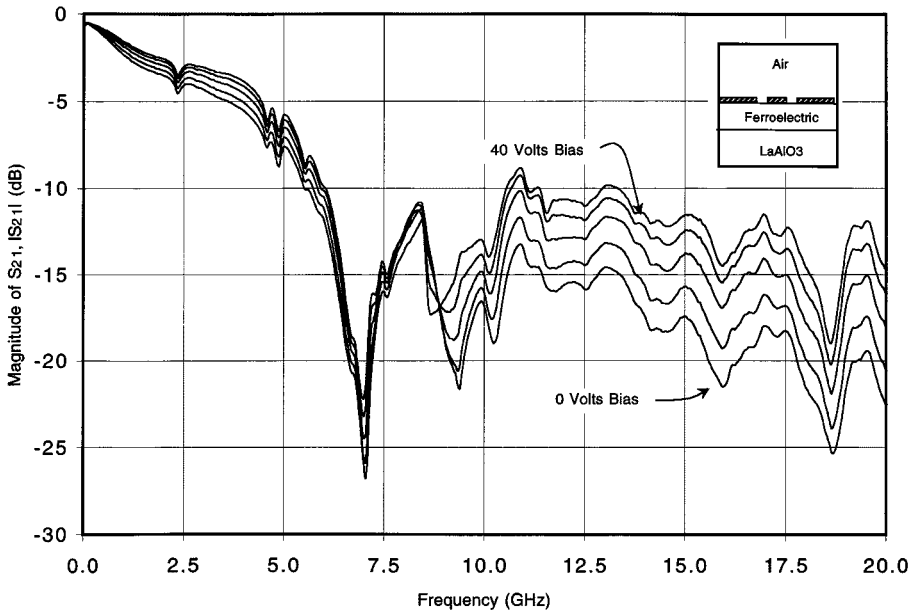

Fig. 9. Corrected insertion loss $|s_{21}|_{\rm corr}$ in decibels, against frequency (in gigahertz) for the $Ba_{0.6}Sr_{0.4}TiO_3$ ferroelectric film over an $LaAlO_3$ substrate. $V_{\rm bias} = 0, 10, 20, 30,$ and 40 V.

for only substrate loss included $\alpha_{\rm sub}$, only the thin-film ferroelectric bulk loss included $\alpha_{\rm fe}$, both of these bulk effects included (lies over the ferroelectric contribution) $\alpha_{\rm sub+fe}$, only the ohmic loss included using the internal self-consistent formula (18) $\alpha_{\rm cond,\,in}$, only the ohmic loss included using the either the external perturbational formulas (22) or (35) with enhancement (39) $\alpha_{\rm cond,\,ext}$, and when all loss mechanisms are included using either the external conductor loss approach $\alpha_{\rm tot,\,ext}$ or the internal loss approach $\alpha_{\rm tot,\,in}$. $w_{\rm eff}$, c_1, f_0 and v in (18) are determined to be $w_{\rm eff} = 3.278$ μm, $c_1 = 1.0$, $f_0 = 10$ GHz and $v = 0.4684$ for Fig. 8(a) when $V_{\rm bias} = 0$ V. $w_{\rm eff}$, c_1, f_0, and v in (18) are determined to be $w_{\rm eff} = 3.394$ μm, $c_1 = 1.0$, $f_0 = 10$ GHz, and $v = 0.3916$ for Fig. 8(b) when $V_{\rm bias} = 40$ V. We see from this figure that use of the external conductor loss perturbational formula (22) leads to over estimation of the total loss in the device, external loss formula (35) leads to both underestimation and overestimation over the frequency band, whereas the internal loss approach correctly models the loss.

For the $LaAlO_3$ substrate device, Fig. 9 gives the corrected insertion-loss measurement, $|s_{21}|_{\rm corr}$ in decibels, over the 0–20-GHz frequency range. Four bias voltage curves are shown, $V_{\rm bias} = 0, 10, 20, 30,$ and 40 V. Loss in the substrate is accounted for by a loss tangent value $\tan\delta = 3.0 \times 10^{-4}$ at room temperature. Fig. 10(a) and (b) provides $\alpha_{\rm exp}$ for the two cases $V_{\rm bias} = 0$ V and 40 V for the $LaAlO_3$ substrate. Here, we also show the theoretical results $[\alpha_{\rm th} = \overline{\alpha}_{\rm th} k_0 (20 \log_{10} e)]$ for the $LaAlO_3$ substrate device, finding $w_{\rm eff} = 2.004$ μm, $c_1 = 1.0$, $f_0 = 10$ GHz, and $v = 0.3727$ for Fig. 10(a) when $V_{\rm bias} = 0$ V. $w_{\rm eff} = 3.021$ μm, $c_1 = 1.0$, $f_0 = 10$ GHz, and $v = 0.3428$ for Fig. 10(b) when $V_{\rm bias} = 40$ V. Notice that, in matching theory to experiment, the questionable excessive excursions between about 5 and 11 GHz of the data was ignored. As in Fig. 8, for the MgO substrate, agreement between theory and experiment is very good for the $LaAlO_3$ substrate device, with use of the external conductor loss perturbational formulas (22) and (35) showing significant discrepancy with frequency from the total device loss. Enhancement (39) was not used because the nominal dielectric constant for the ferroelectric film was so much larger than either the substrate or air region above the device surface, and it caused $\alpha_{\rm cond,ext}$ to be a factor of five or more below the experimental results. Instead

$$\varepsilon_{re} = \varepsilon_{xx}. \tag{42}$$

When the conductor loss is taken into account by simultaneously satisfying $\beta_{\rm th}[\varepsilon(0);\, w_{\rm eff},\, c_1,\, v] = \beta_{\rm exp}$, and $\alpha_{\rm th}[\varepsilon(0);\, w_{\rm eff},\, c_1,\, v] = \alpha_{\rm exp}$ or $\beta_{\rm th}[\varepsilon_{xx}(E_{x,\rm bias});\, w_{\rm eff},\, c_1,\, v] = \beta_{\rm exp}$ and $\alpha_{\rm th}[\varepsilon_{xx}(E_{x,\rm bias});\, w_{\rm eff},\, c_1,\, v] = \alpha_{\rm exp}$ under bias, it allows revised unbiased scalar permittivity values and permittivity tensors to be found. (Before in obtaining (18), only $\alpha_{\rm th}[w_{\rm eff},\, c_1,\, v] = \alpha_{\rm exp}$ was examined, which is reasonable for low-loss devices. Permittivity extraction in Section IV was done by using only $\beta_{\rm th}[\varepsilon(0)] = \beta_{\rm exp}$ or $\beta_{\rm th}[\varepsilon_{xx}(E_{x,\rm bias})] = \beta_{\rm exp}$). For the MgO substrate device, for $V_{\rm bias} = 0$ V, it has the same slowing value as before $\overline{\beta} = 3.614$, with $\overline{\alpha} = 0.2510$ (attenuation now included at 10 GHz) with a new scalar permittivity value of $\varepsilon(0) = 101.5 - i101.5 \tan\delta_{\rm fe}$. Under bias $V_{\rm bias} = 40$ V, $\overline{\beta} = 3.413$ (unchanged from the lossless value since it must agree with experiment), $\overline{\alpha} = 0.2298$ (at 10 GHz), and yields a new MgO device permittivity tensor $\overline{\overline{\varepsilon}}$ of

$$\overline{\overline{\varepsilon}}(V_{\rm bias} = 40\ {\rm V}) = \begin{bmatrix} 75.27 & 0 & 0 \\ 0 & 101.5 & 0 \\ 0 & 0 & 101.5 \end{bmatrix} - i \begin{bmatrix} 75.27 & 0 & 0 \\ 0 & 101.5 & 0 \\ 0 & 0 & 101.5 \end{bmatrix} \tan\delta_{\rm fe}. \tag{43}$$

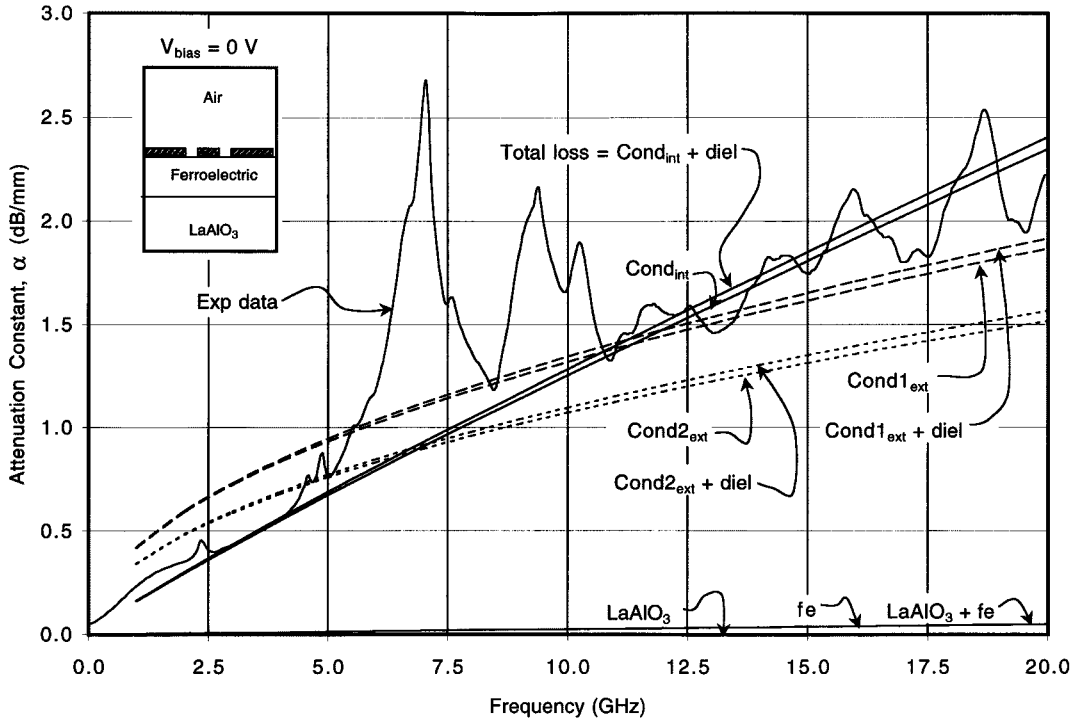

(a)

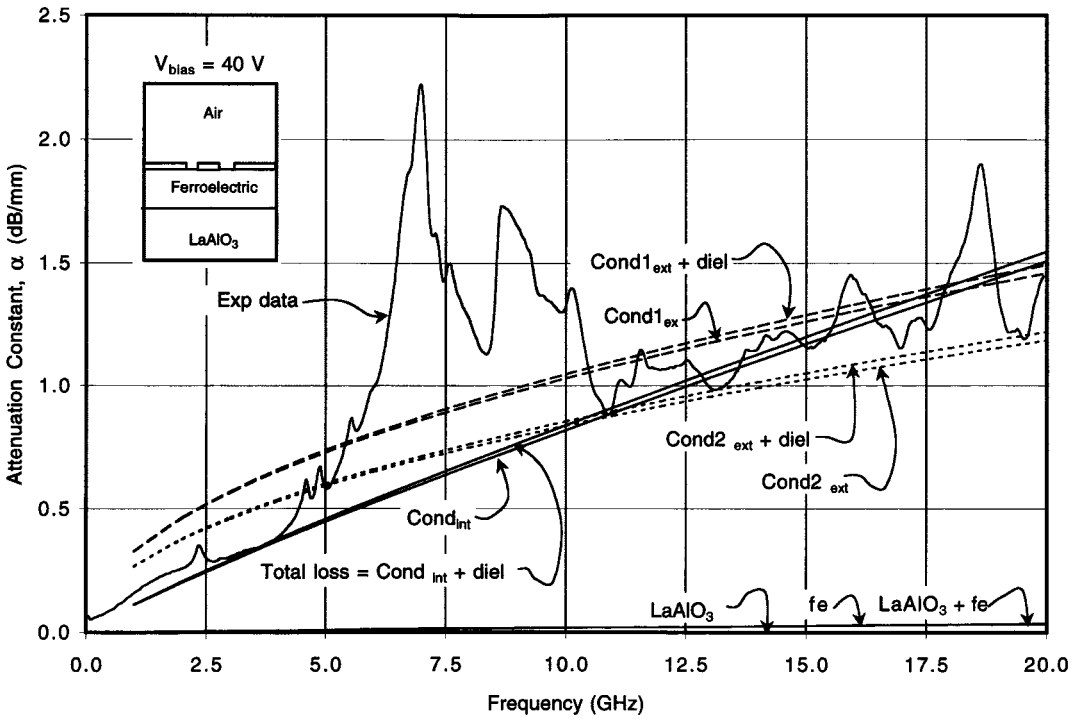

(b)

Fig. 10. Laboratory measured $\alpha_{\exp}$ is plotted for the two cases: (a) $V_{\text{bias}} = 0$ V and (b) 40 V for the $Ba_{0.6}Sr_{0.4}TiO_3$ ferroelectric film over an $LaAlO_3$ substrate. Theoretical attenuative results [$\alpha_{\text{th}} = \overline{\alpha}_{\text{th}} k_0 (20 \log_{10} e)$] are shown too for only substrate loss α_{sub}, thin-film ferroelectric bulk loss α_{fc}, both of these bulk effects $\alpha_{\text{sub+fc}}$, only the ohmic loss using the internal self-consistent formula (18) $\alpha_{\text{cond, in}}$, only the ohmic loss using either of the external perturbational formulas (22) or (35) $\alpha_{\text{cond,ext}}$, total loss $\alpha_{\text{tot, ext}}$, which includes the ohmic loss using either of the external perturbational formulas (22) or (35) and both the dielectric layer loss parts, and the total loss $\alpha_{\text{tot, in}}$, which includes the ohmic loss using the internal self-consistent formula (18) and both the dielectric layer loss parts.

These permittivity changes are seen to be significant (for the real part of the above expression) compared to the lossless case, and providing some noticeable fraction of phase slowing (and, thus, phase-shifting characteristics) because, in the ferroelectric device, large fields exist around the slots, say, compared to a lower loss microstrip configuration. For the $LaAlO_3$ substrate

device, for $V_{\text{bias}} = 0$ V, it has $\overline{\beta} = 5.110$ (same as the lossless value), $\overline{\alpha} = 0.6808$ (at 10 GHz) with a new scalar permittivity value of $\varepsilon(0) = 440.0 - i440.0 \tan \delta_{\text{fe}}$. Under bias $V_{\text{bias}} = 40$ V, $\overline{\beta} = 4.576$, $\overline{\alpha} = 0.4612$ (at 10 GHz), and yields a new $LaAlO_3$ device permittivity tensor $\overline{\overline{\varepsilon}}$ of

$$\overline{\overline{\varepsilon}}(V_{\text{bias}} = 40\text{ V}) = \begin{bmatrix} 187.4 & 0 & 0 \\ 0 & 440.0 & 0 \\ 0 & 0 & 440.0 \end{bmatrix} - i \begin{bmatrix} 187.4 & 0 & 0 \\ 0 & 440.0 & 0 \\ 0 & 0 & 440.0 \end{bmatrix} \tan \delta_{\text{fe}}. \quad (44)$$

For both the MgO and $LaAlO_3$ cases, the G_{s3} (the dyadic modifying term) was amended by another term G_{s3a} to perform the extraction process (while avoiding redetermining w_{eff}, c_1, v) because of the significant loss of these devices. Thus, the total dyadic modifying impedance is $G_{s3T} = G_{s3} + G_{s3a}$. For MgO, $G_{s3T} = (0.0213, 0.0137)\ \Omega$ at $V_{\text{bias}} = 0$ V with $G_{s3a} = (0.0001, -0.0074)\ \Omega$. At $V_{\text{bias}} = 40$ V for MgO, $G_{s3T} = (0.0217, 0.0187)\ \Omega$ with $G_{s3a} = (-0.0022, -0.0052)\ \Omega$. The $LaAlO_3$ substrate structure has $G_{s3T} = (0.2084, 0.1122)\ \Omega$ with $G_{s3a} = (-0.0035, -0.0997)\ \Omega$ at $V_{\text{bias}} = 0$ V, and $G_{s3T} = (q = 0.1663, m = 0.1543)\ \Omega$ with $G_{s3a} = (q - 0.1405, m - 0.1405)\ \Omega$ at $V_{\text{bias}} = 40$ V.

VI. Conclusion

A theoretical procedure for determining the permittivity properties of thin-film ferroelectric devices has been presented. This procedure is to be used in conjunction with a full-wave field solver for extracting the isotropic and anisotropic behavior of the thin ferroelectric film. A full-wave spectral-domain integral-equation code with an anisotropic Green's function has been used to find the permittivity values for two ferroelectric thin-film devices operated in the microwave frequency regime. Tensor solutions for these devices have been given.

In addition, the various loss contributions have been assessed, including the ohmic (conductor loss) contribution that is dominant. Substrate and ferroelectric bulk loss, characterized by a loss tangent, are treated in a fully self-consistent way in the Green's function construction. Ohmic loss, by the interfacial guiding coplanar metal, was handled in one of the following basic ways: 1) dyadic Green's function element modification within the self-consistent process or 2) attenuation constant modification by adding in the ohmic loss perturbationally part after the self-consistent process was completed.

Both ferroelectric devices, although containing loss, only had minor changes to their phase propagation properties when loss was added. Thus, the device operation is controlled by the ferroelectric permittivity tensor behavior, and not the loss.

Acknowledgment

The authors would like to thank Dr. S. A. Wolf, Defense Advanced Research Project Agency (DARPA), Arlington, VA, for encouraging this paper's research.

References

[1] S. W. Kirchoefer, J. M. Pond, A. C. Carter, W. Chang, K. K. Agarwal, J. S. Horwitz, and D. B. Chrisey, "Microwave properties of $Sr_{0.5}Ba_{0.5}TiO_3$ thin-film interdigitated capacitors," *Microwave Opt. Technol. Lett.*, vol. 18, pp. 168–171, June 1998.

[2] S. W. Kirchoefer, J. M. Pond, H. S. Newman, W.-J. Kim, and J. S. Horwitz, "Ferroelectric/ferrite tunable phase shifters," in *IEEE MTT-S Int. Microwave Symp. Dig.*, vol. 3, June 2000, pp. 1359–1362.

[3] F. W. Van Keuls, C. H. Mueller, F. A. Miranda, R. R. Romanofsky, C. L. Canedy, S. Aggarwal, T. Venkatesan, R. Ramesh, J. S. Horwitz, W. Chang, and W. J. Kim, "Room temperature thin film $Ba_xSr_{1-x}TiO_3$ Ku-band coupled microstrip phase shifters: Effects of film thickness, doping, annealing and substrate choice," in *IEEE MTT-S Int. Microwave Symp. Dig.*, vol. 2, June 1999, pp. 737–740.

[4] C. M. Krowne, "Fourier transformed matrix method of finding propagation characteristics of complex anisotropic layered media," *IEEE Trans. Microwave Theory Tech.*, vol. MTT-32, pp. 1617–1625, Dec. 1984.

[5] A. A. Mostafa, C. M. Krowne, and K. A. Zaki, "Numerical spectral matrix method for propagation in general layered media: Application to isotropic and anisotropic substrates," *IEEE Trans. Microwave Theory Tech.*, vol. MTT-35, pp. 1399–1407, Dec. 1987.

[6] C. M. Krowne, "Theoretical considerations for full-wave electromagnetic-media interactions in layered structures with ferroelectric or ferromagnetic materials," *Proc. SPIE–Int. Soc. Opt. Eng.*, vol. 4097, pp. 70–84, July 30, 2000.

[7] ——, "Theoretical considerations for finding anisotropic permittivity in layered ferroelectric/ferromagnetic structures from full-wave electromagnetic simulations," *Microwave Opt. Technol. Lett.*, vol. 28, pp. 63–69, Jan. 2001.

[8] C. M. Krowne, S. W. Kirchoefer, and J. M. Pond, "Anisotropic permittivity extraction from phase propagation measurements using an anisotropic full-wave Green's function solver for coplanar ferroelectric thin film devices," in *IEEE MTT-S Int. Microwave Symp. Dig.*, vol. 2, June 2000, pp. 1193–1196.

[9] C. M. Krowne, "Nonlinear electromagnetic wave propagation in ferroelectric integrated structures," *Microwave Opt. Technol. Lett.*, vol. 17, pp. 213–225, Feb. 1998.

[10] ——, "Full-wave spectral Green's function integral equation calculation of coplanar ferroelectric thin film transmission structures," *Microwave Opt. Technol. Lett.*, vol. 26, no. 3, pp. 187–192, Aug. 2000.

[11] D. Mirshekar-Syahkal, "An accurate determination of dielectric loss effect in monolithic microwave integrated circuits including microstrip and coupled microstrip lines," *IEEE Trans. Microwave Theory Tech.*, vol. MTT-31, pp. 950–954, Nov. 1983.

[12] C. M. Krowne, "Microstrip conductor losses calculated by full wave and perturbational approaches," *Electron. Lett.*, vol. 24, no. 9, pp. 552–553, Apr. 1988.

[13] J. M. Pond, C. M. Krowne, and W. L. Carter, "On the application of complex resistive boundary conditions to model transmission lines consisting of very thin superconductors," *IEEE Trans. Microwave Theory Tech.*, vol. 37, pp. 181–190, Jan. 1989.

[14] E. Paleczny, D. Kinowski, J. F. Legier, P. Pribetich, and P. Kennis, "Comparison of full wave approaches for determination of microstrip conductor losses for MMIC applications," *Electron. Lett.*, vol. 26, no. 25, pp. 2076–2077, Dec. 1990.

[15] M. E. Goldfarb and A. Platzker, "Losses in GaAs microstrip," *IEEE Trans. Microwave Theory Tech.*, vol. 35, pp. 1957–1963, Dec. 1990.

[16] C. M. Krowne, "Relationships for Green's function spectral dyadics involving anisotropic imperfect conductors imbedded in layered anisotropic media," *IEEE Trans. Antennas Propagat.*, vol. 37, pp. 1207–1211, Sept. 1989.

[17] K. C. Gupta, R. Garg, and R. Chadha, *Computer Aided Design of Microwave Circuits*. Norword, MA: Artech House, 1981.

[18] K. C. Gupta, R. Garg, and I. J. Bahl, *Microstrip Lines and Slotlines*, 2nd ed. Norword, MA: Artech House, 1996.

Clifford M. Krowne (S'73–M'74–SM'83) received the B.S. degree in physics from the University of California at Berkeley and Davis, in 1970, and the M.S. degree and Ph.D. degree (solid-state transport, many body scattering) from the University of California at Los Angeles, in 1972 and 1975, respectively.

He was with the Microelectronics Division, Lockheed Missiles and Space Company, Sunnyvale, CA. He was a Member of the Solid-State Technical Staff of the Watkins-Johnson Company, Palo Alto, CA. He was a faculty member in the Department of Electrical Engineering, North Carolina State University, Raleigh. He was also an Adjunct Professor of electrical engineering at the University of Maryland at College Park. Since 1982, he has been with the Microwave Technology Branch, Electronics Science and Technology Division, Naval Research Laboratory, Washington, DC, where he has been involved in the study of microwave and millimeter-wave properties of active and passive solid-state devices. He has authored or co-authored 170 conference and journal papers in solid-state electronics, microwave circuits, electromagnetics, and physics. He holds several patents. He has also written major portions of four books in the "Advances in Imaging and Electron Physics Series" on propagation in anisotropic media and circulation behavior in nonreciprocating media (New York: Academic, 1995, vol. 92; 1996, vol. 98; 1998, vol. 103; 1999, vol. 106), and has also made a contribution on numerical modeling of microstrip circulators in the ferrite devices area for the *Electrical and Electronics Engineering Encyclopedia* (New York: Wiley, 1999). He is listed in *Who's Who in Frontiers of Science and Technology*, *Who's Who in the World*, and *Who's Who in Electromagnetics*.

Dr. Krowne is a member of Phi Kappa Phi, Tau Beta Pi, and the American Physical Society. He is a Fellow of the Washington Academy of Sciences. He has served on the Technical Program Conference Committees of the IEEE Antennas and Propagation Society (IEEE AP-S) (1983, 1984) and the IEEE Microwave Theory and Techniques Society (IEEE MTT-S) (1982–1996). He has chaired sessions in the electromagnetic theory, microstrip antenna, and solid-state devices/circuits, superconductor, and monolithic circuit areas, and has organized two IEEE MTT-S workshops on two-dimensional (2-D)/three-dimensional (3-D) full-wave simulation (1992) and self-consistent particle transport/full-wave dynamic field simulation (1993). He was a member of the 1987 IEEE MTT-S Symposium Steering Committee.

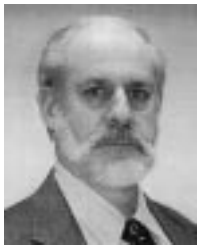

Maurice Daniel received the B.S. degree in physics from Case Western Reserve University, Cleveland, OH, in 1965, and the M.B.A. degree from George Washington University, Washington, DC, in 1998.

From 1965 to 1975, he was an Assembly Language Programmer at the Fairchild Hiller Corporation (supporting NASA), Information Networks Division, General Electric, RCA Corporation, U.S. Navy Underwater Testing Range, and Input/Output Computer Services Inc. (in support of the Massachusetts Institute of Technology (MIT) Lincoln Laboratory). He has performed a variety of engineering and tasks from the late 1970s to 1980s. He co-founded Lumitex Inc., Cleveland, OH, to manufacture light-emitting panels based on his patents. He has been with the DCS Corporation, Alexandria, VA, for the last 15 years in support of various Navy projects. He has provided laboratory support to the Naval Research Laboratory since 1995, including work on the software design, coding, and application of the microwave transmission-line structure model. He has authored over 50 technical papers internal to the U.S. Government. He has 16 patents issued or pending on optical devices and aerospace hardware.

Dr. Daniel is an active member of the Inventors Network of the Capital Area (INCA) and the MIT Forum.

Steven W. Kirchoefer (S'80–M'82) received the B.S., M.S., and Ph.D. degrees from the University of Illinois at Urbana-Champaign, in 1978, 1979, and 1982, respectively, all in electrical engineering.

Since 1982 he has been with the U.S. Naval Research Laboratory, Washington, DC, where he has been involved in the application of compound semiconductors and other materials for high-speed devices. He has fabricated and demonstrated a wide variety of prototype device concepts, including semiconductor quantum-well devices utilizing real space transfer, and confined particle effects. He has recently been involved with the characterization of microwave properties of ferroelectric thin films, which includes the study of interdigitated capacitors for varactor applications, as well as the fabrication and measurement of distributed coplanar-waveguide structures for phase-shifter applications.

Jeffrey M. Pond (M'81) was born in South Haven, MI, on April 10, 1956. He received the B.S. degree in electrical engineering from Michigan State University, East Lansing, in 1978, and the M.S. and Ph.D. degrees in electrical engineering from The University of Michigan at Ann Arbor, in 1979 and 1982, respectively.

While at The University of Michigan at Ann Arbor, he was a Graduate Research Assistant in the Radiation Laboratory. In September 1982, he joined the Electronics Science and Technology Division, Naval Research Laboratory, Washington, DC, where he is a member of the Microwave Technology Branch's Solid-State Circuits Section. His research interests have included microwave cryogenic measurements, cryogenic microwave electronics, microwave applications and measurements of low- and high-temperature superconductors, and ferroelectric materials for microwave applications. His current major research focus is on novel compact microwave resonator and filter concepts. He has authored or co-authored over 100 journal papers and conference presentations. He holds several patents.

Dr. Pond is a member of the IEEE Microwave Theory and Techniques Society (IEEE MTT-S) and the IEEE Antennas and Propagation Society (IEEE AP-S). In 2000, he served as the secretary of the IEEE MTT-S and is currently a member of the IEEE MTT-S AdCom. He has been an active member of the Steering Committees for the 1998 IEEE International Microwave Symposium (IMS), Baltimore, MD, the 2000 IEEE IMS, Boston, MA, and the 2001 IEEE IMS, Phoenix), AZ. He is also involved in web sites in support of the IEEE IMS and other technical conferences.